J Braz. Soc. Mech. Sci. Eng. (2016) 38:773–787
DOI 10.1007/s40430-014-0285-1

TECHNICAL PAPER

Acoustic simulation of scattering sound from a more realistic sea surface: consideration of two practical underwater sound sources

Parviz Ghadimi · Alireza Bolghasi · Mohammad A. Feizi Chekab

Received: 20 March 2014 / Accepted: 18 November 2014 / Published online: 14 December 2014

Abstract A computer program named sea surface acoustic simulator (SSAS) is developed based on an optimized Helmholtz–Kirchhoff–Fresnel method. This software is capable of simulating the scattering properties of incident sound from the sea surface under the combined effect of surface roughness and subsurface bubbles. The scattered sound pressure level, sound intensity and scattering coefficient are some outputs of this simulator under different environmental conditions and source features. Two different sound sources are considered in the current study. In the first case, sound is generated by an explosion and the developed software is validated by CST experiments which use explosive charges as sound sources. Accordingly, one of these explosions is simulated by the program and the resulting scattering coefficient is compared against CST7 experimental data. In the second case, hydrodynamic pressure of a moving submerged object considered as a sound source, is investigated. Hydrodynamic pressure is calculated by COMSOL Multiphysics 4.3 software and the numerical findings are used as input data for the introduced acoustic simulator. Three-dimensional scattered acoustic pressure level (dB) is calculated by SSAS program and presented for both cases.

Keywords Sea surface acoustic simulator · Sea surface · Scattering coefficient · Pressure level

List of symbols

f	Frequency
ω	Angular frequency of sound
$\mathcal{R}$	Reflection coeff. (sea to bubbly water)
$\mathcal{R}_{13}$	Reflection coeff. (water to air)
k	Sound wave number
c	Sound speed
ρ_1	Water density
ρ_2	Bubbly water density
z	Bubbly water depth
ρ_3	Air density
C_1	Sound speed in water
C_2	Sound speed in bubbly water
C_3	Sound speed in air
R_s	Source location
W	Wind speed
N	Bubble population
X	Position vector
P_Final	Scattered pressure level (dB)

1 Introduction

Effects of sea surface on the incident sound have been examined by different acousticians due to their important role on sound propagation and reverberation [1]. After Second World War, these studies have been pursued, more seriously. Marsh [2] developed a general theory of scattering from irregular surfaces and using a suitable mathematical calculation of the sea surface, qualitative account of reverberation was presented. Kou [3] developed Marsh's perturbation method and proved the usefulness of Marsh–Kuo's perturbation method by comparing his results against experimental data. Another type of perturbation method was suggested by Bass [4] which divides a velocity

Technical Editor: Fernando Alves Rochinha.

P. Ghadimi (✉) · A. Bolghasi · M. A. Feizi Chekab
Department of Marine Technology, Amirkabir University of Technology, Hafez Ave, No 424, P.O. Box 15875-4413, Tehran, Iran
e-mail: pghadimi@aut.ac.ir

potential field into the mean and scattered velocity potential fields. His method resulted in a specular reflection process which satisfies the conservation of energy, approximately. Another approach was reported by Brekhovskikh and Lysanov [5] which is a simple method and physically appealing. Brekhovskikh and Lysanov [5] and Marsh et al. [6] went beyond the perturbation approximation to get a closed-form solution for the scattering loss. All the mentioned schemes using perturbation method such as joint surface roughness and/or volumetric perturbation scattering theory proposed by Kuo [7] can examine the scattering of an incident sound from the ocean surface by considering the important physical factors involved in sound quality variation. However, most of the developers of these techniques were forced to make some drastic assumptions and/or use some empirical relations for solving the derived equations. For example, Kuo [7] used the Pierson and Moskowitz wave spectrum in obtaining the required rough sea surface spectrum that can not be considered a comprehensive approach.

An alternative method for acoustic modeling of the sea surface which considers the pressure nature of the sound and forms the core of mathematical physics of sound propagation is based on the Rayleigh, Helmholtz, Kirchhoff, Born, and Fresnel classical techniques. These classical techniques can be used in different numerical models to simulate the sea surface effects on incident sound. Helmholtz–Kirchhoff–Fresnel (HKF) integral is one of these models which can calculate the scattered pressure field as a function of frequency [8] as in

$$P(f) \approx \frac{iP_0R_0\mathcal{R}k(\cos\psi_1+\cos\psi_2)e^{-ik(R_1+R_2)}}{4\pi R_1R_2}\int_{-x_1}^{x_1}\mathrm{d}x'\int_{-y_1}^{y_1} \times D\ \exp\left\{-i\left[\frac{x'^2}{x_f^2}+\frac{y'^2}{y_f^2}+kx(\sin\psi_1-\sin\psi_2\cos\psi_3)-ky'\sin\psi_2\sin\psi_3+k\xi(\cos\psi_1+\cos\psi_2)\right]\right\}\mathrm{d}y' \tag{1}$$

where

$$x_f^{-2} \equiv \frac{k}{2}\left(\frac{\cos^2(\psi_1)}{R_1}+\frac{1-\sin^2(\psi_2)\cos^2(\psi_3)}{R_2}\right) \tag{2}$$

$$y_f^{-2} \equiv \frac{k}{2}\left(\frac{1}{R_1}+\frac{1-\sin^2(\psi_2)\sin^2(\psi_3)}{R_2}\right) \tag{3}$$

Based on Eq. (1), it is possible to calculate the scattered sound from a rough sea surface for a source with known features like position vector (X), incident angle to the sea surface (ϕ_i), frequency (f), and source pressure (P_0) at a range R_0 with source directionality D. The scattered sound can be calculated at any point in the upper medium by inserting the value of its position vector (R_2) and its angle related to the struck point on the rough surface in Eq. (1). Other involved parameters are identified in Fig. 1.

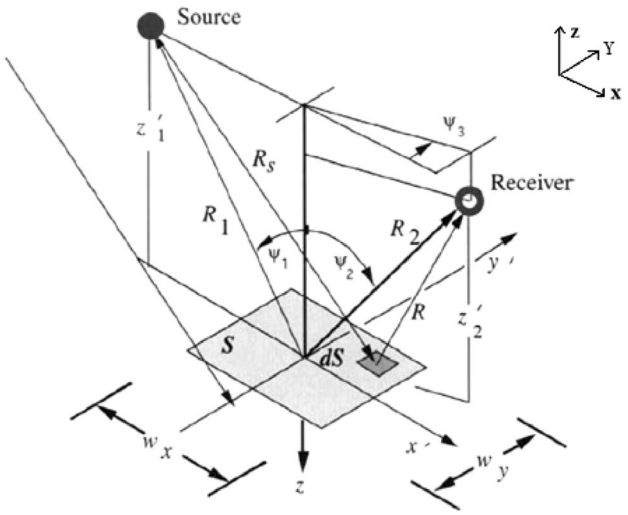

Fig. 1 The considered geometry and definition of parameters in HKF method [8]

Using Eq. (1), it is possible to calculate the scattered field from the rough sea surface, but there is another important factor which can affect the incident sound [8]. This factor is sub-surface bubbles cloud which becomes more important in higher frequencies and at high wind speeds [9]. In the real sea condition, due to the presence of wind and resulting waves on the sea surface, there are bubble clouds under the sea surface which are generated by the breaking waves. Different acousticians have studied the influence of bubbles on sound scattering. McDonald [10], Henyey [11], Medwin [12], Prosperetti et al. [13], Hall [14], Fialkowski, and Gauss [15] have examined the sound propagation in bubbly water using various methods. These methods take different approaches into account to study the sound variation in bubbly water. For instance, Prosperetti et al. [13] proposed the natural sound-producing mechanisms at frequencies between 20 and 500 Hz as a result of wave-turbulence interactions and oscillating bubble clouds. In another work, depth dependence of bubbly layer effect on attenuation of the incident sound was also examined by Medwin and Clay [8], which was considered to be a non-ignorable factor. On the other hand, different physical factors were considered for bubble generation by acousticians,

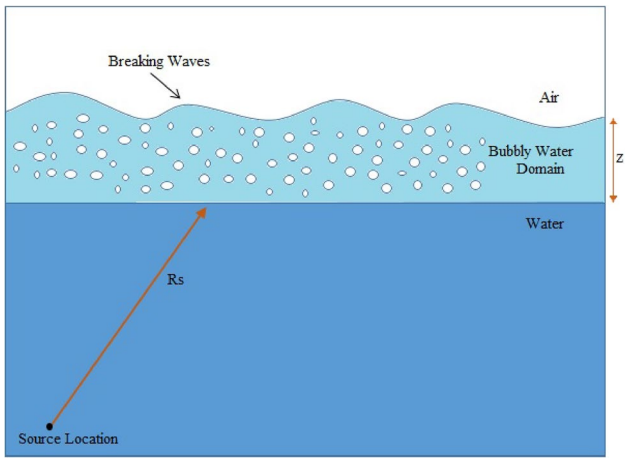

Fig. 2 Schematic of the optimized HKF (O-HKF) method

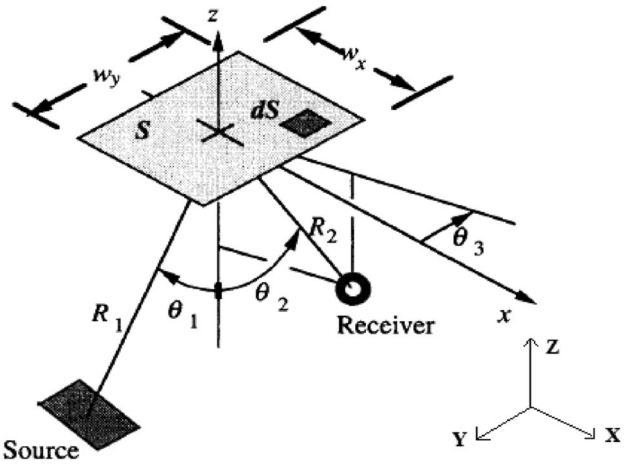

Fig. 3 Scattering geometry: dS is differential area of height ξ with respect to the mean surface [8]

like rainfall by Medwin et al. [16] and breaking waves by Hall [14].

It is quite apparent from the foregoing discussion that, to simulate the acoustic effects of sea surface more accurately, it is essential to present a model which can cover the bubbles effects, as well. It is for this reason that the new optimized HKF method has been developed and presented in this paper.

2 Optimized Helmholtz–Kirchhoff–Fresnel (O-HKF) method

As pointed out earlier, most of the researchers in the past have made different simplifying assumptions for examining the sound scattering. These assumptions have caused some errors in the conducted numerical and empirical studies. Consideration of a smooth interface between the air and water, neglecting the bubble cloud effects, and studying the sound scattering only as a function of the impedance are some of these assumptions. Although, methods like HKF can analyze the surface scattering by a rough interface, it may still cause undesirable error due to neglecting of the sub-surface bubble cloud effect. Therefore, it becomes necessary to optimize the HKF method for analyzing the sound scattering. Accordingly, a third phase called the bubbly water medium must be added to the previous phases of air and water in the original HKF method for improving the determination of the sound scattering. This was accomplished by introducing a reflection coefficient $\mathcal{R}_{13}$ given in Eq. (4) into Eq. (1). Figure 2 indicates that when an incident sound strikes the sea surface, it will face a three phase region with different impedances and a rough interface between the air and bubbly water media. Reflection coefficient $\mathcal{R}_{13}$ can be defined for a multi layers region as

$$\mathcal{R}_{13} = \frac{\mathcal{R}_{12} + \mathcal{R}_{23}\exp(-i2\phi_2)}{1 + \mathcal{R}_{12}\mathcal{R}_{23}\exp(-i2\phi_2)} \tag{4}$$

where ϕ_2 is

$$\phi_2 = k_2 z\ \cos\theta_2 \tag{5}$$

where k_2 is the wavenumber in the bubbly water.

If Eq. (4) is substituted into Eq. (1) as a reflection coefficient, the resulting equation can be used to calculate the scattered field from a sea surface which includes the influence of both surface roughness and sub-surface bubbles. This model is called optimized HKF (O-HKF) method and is used to develop the proposed sea surface acoustic simulator (SSAS) software.

2.1 Derivation of the optimized-HKF integral

If the incident sound is considered as

$$p_{\text{inc}} = \frac{D_t P_0 R_0 \exp[i(\omega t - kR_s)]}{R_s}, \tag{6}$$

Equation (1) can then be written as

$$p \cong \frac{ip_0 R_0 \mathcal{R}_{13} kG(\theta)\exp[i\omega t - ik(R_1 + R_2)]}{2\pi R_1 R_2} \times \int_{-\infty}^{\infty}\int D_t \exp\left[-i\left(\frac{x^2}{x_f^2} + \frac{y^2}{y_f^2} + 2\alpha x + 2\beta y + 2\gamma\xi\right)\right]\mathrm{d}y\mathrm{d}x \tag{7}$$

where

$$G(\theta) \cong \frac{\cos\theta_i + \cos\theta_2}{2} \tag{8}$$

$$2\alpha \equiv k(\sin\theta_i - \sin\theta_2\cos\theta_3) \tag{9}$$

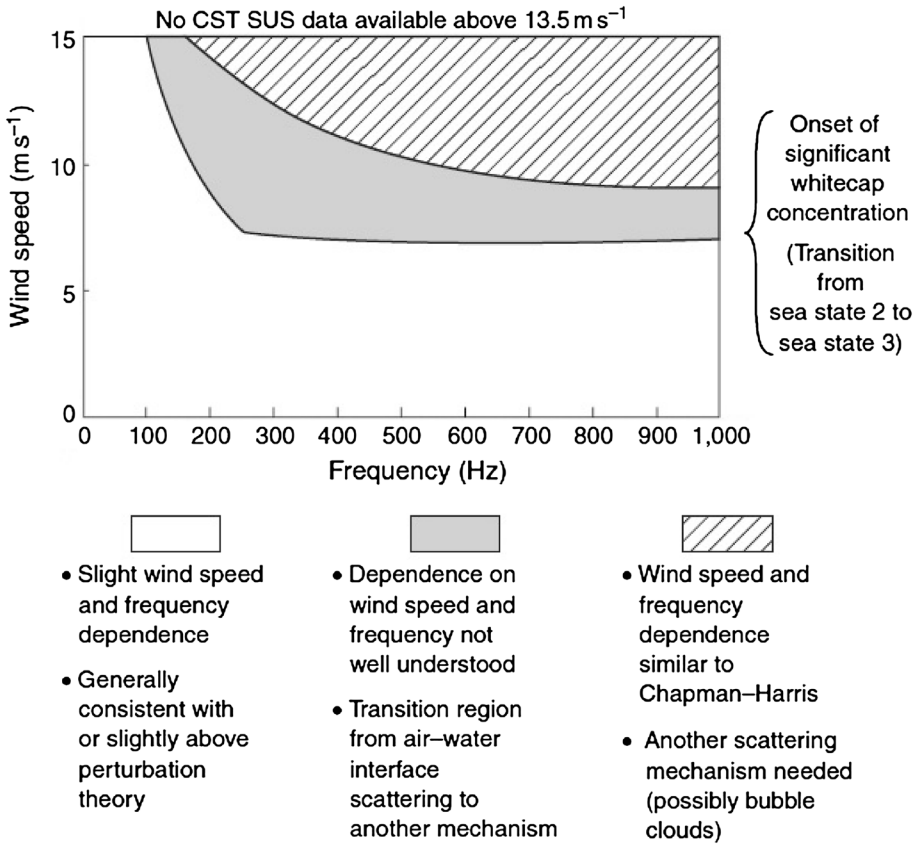

Fig. 4 Frequency wind speed ($f-U$) domain for the sea-surface scattering strengths [9]

Table 1 Summary of the selected CST7 runs [17]

Run	Receiver depth (m)	Estimated SUS detonation depth (m)	Average wind speed (m/s)	Relative wind direction (deg.)	Significant wave height (m)	Estimated sea state
3C	160	540	15.0	158	3.0	4
16G	220	600	15.5	346	4.9	6
25D	177	550	3	269	2.2	2

$$2\beta \equiv -k(\sin\theta_2 \sin\theta_3) \tag{10}$$

$$2\gamma \equiv k(\cos\theta_i + \cos\theta_2) \tag{11}$$

Here, θ_2 is the receiver position vector related to z axis, θ_3 is the receiver's plane angle related to z axis, shown in Fig. 3.

To solve the integral in Eq. (7), two different terms for the sea surface can be considered. First term is related to the surface roughness which is defined by Medwin and Clay [8] as

$$\mathcal{W} = \langle \exp[2i\gamma(\xi - \xi')] \rangle = \int_{-\infty}^{\infty}\int_{-\infty}^{\infty} w_2 \exp\left[2i\gamma(\xi - \xi')\right] \mathrm{d}\xi \mathrm{d}\xi' \tag{12}$$

where w_2 is the bivariate probability density function (PDF) that is defined as

$$w_2(x, y, x+\xi, y+\eta) \equiv \left[2\pi h^2 \left(1 - C^2\right)^{\frac{1}{2}}\right]^{-1} \exp\left\{-\frac{\xi_1^2 + \xi_2^2 - 2\xi_1\xi_2 C}{2h^2(1-C^2)}\right\} \tag{13}$$

Here, C is the correlation of the surface heights which is defined as follows:

$$C = \frac{\langle \xi_1 \xi_2 \rangle}{h^2} \tag{14}$$

Second term is related to the beam geometry that shows the source and the receiver positions related to the sea surface and is defined as

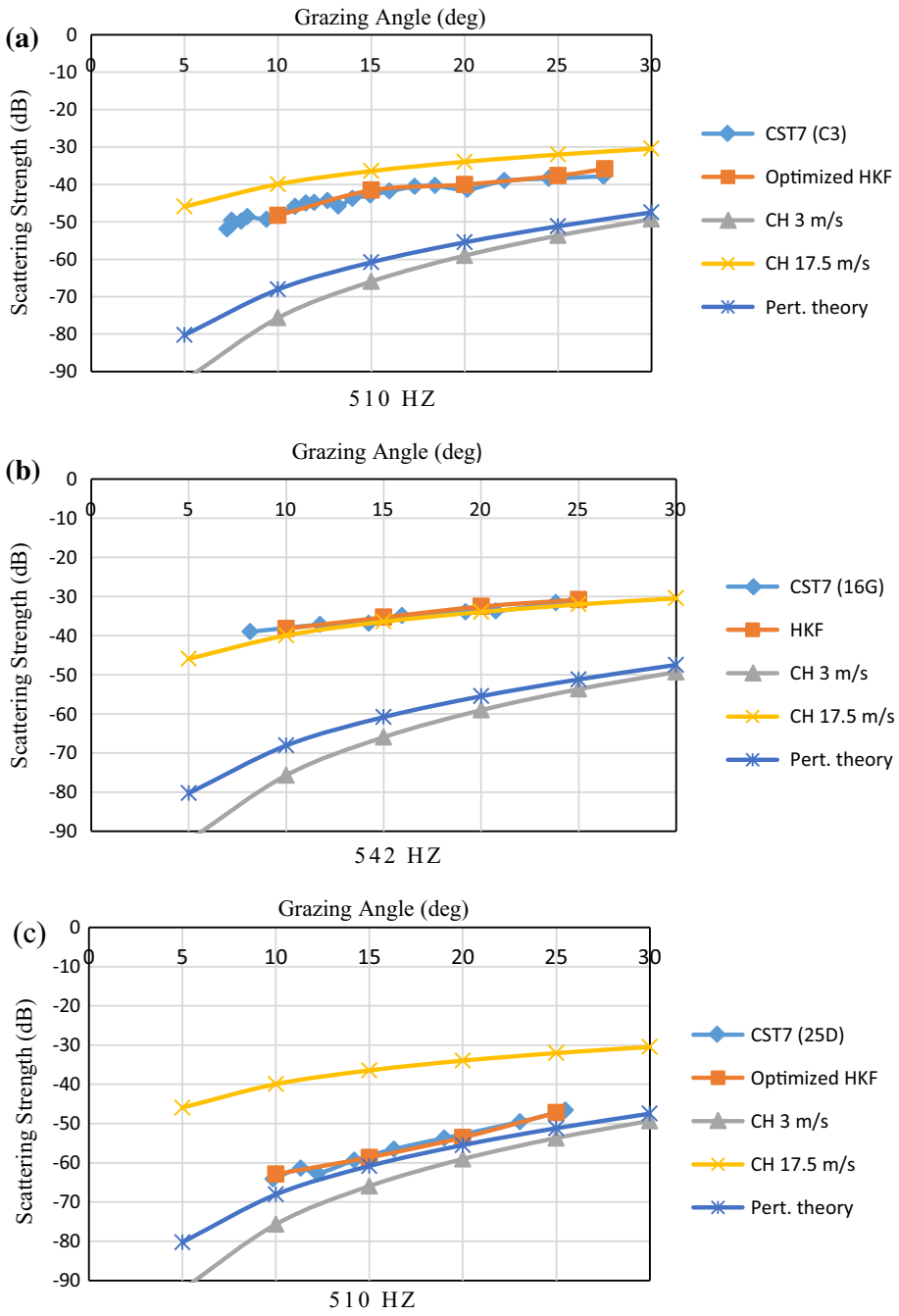

Fig. 5 Results of the scattering strengths by the optimized HKF method compared against CH, perturbation theory and **a** CST7 (3C), **b** CST7 (16G), **c** CST7 (25D)

$$\mathcal{G}\exp\left(2i\alpha\xi + 2i\beta\eta\right) \tag{15}$$

where

$$\mathcal{G} \equiv \exp(-a_\xi \xi^2 - a_\eta \eta^2) \tag{16}$$

In this equation, a_ξ and a_η can be obtained by Eqs. (17) and (18):

$$a_\xi = \frac{X^2}{2x_f^4} + \frac{1}{2X^2} \tag{17}$$

$$a_\eta = \frac{Y^2}{2y_f^4} + \frac{1}{2Y^2} \tag{18}$$

Using Eqs. (12) and (15), the integral in Eq. (7) can be defined in the following form:

$$p = p_0^2 R_0^2 \frac{\mathcal{R}_{13}^2 K^2 G^2(\theta) A e^{i\omega\tau}}{8\pi^2 R_1^2 R_2^2} \int_{\infty}^{\infty}\int GW e^{2i(\alpha\xi+\beta\eta)}\,\mathrm{d}\xi\,\mathrm{d}\eta \tag{19}$$

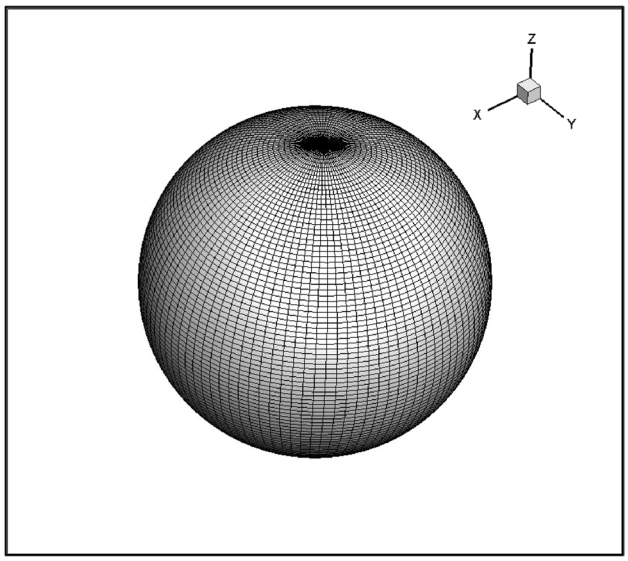

Fig. 6 Discretized domain in spherical coordinates

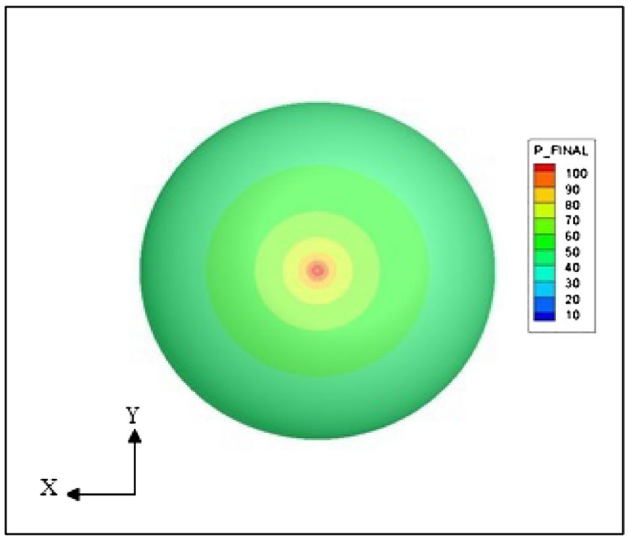

Fig. 7 CST7 explosion pressure field (dB)

Using Eq. (19), it is possible to calculate the scattered sound from the rough sea surface including the sub-surface bubble effect. Equation (19) presents the scattered pressure by the optimized HKF method.

3 Experimental test cases as bases of comparison

In the previous section, the O-HKF method and its features for determining the sound scattering were discussed. Since O-HKF method considers wider range of important physical factors, it will be more practical to examine the sound scattering from the rough ocean surface with sub-surface bubbles by this method. In the meantime, its results can be compared against experimental data such as the critical sea tests (CST) conducted by Ogden and Erskine [9, 17]. Ogden and Erskine [9], through the CST experiments, concluded that there are two different mechanisms which can affect sound scattering from the sea surface. One mechanism depends on the surface roughness and the other is related to the sub-surface bubbles. They also concluded that there is a transition area in which both bubbles and surface roughness should be included as demonstrated in Fig. 4. Since the optimized KHF method can cover bubbles and surface roughness effects, its scattering results can be confidently compared with the CST runs. To validate the results of the developed SSAS program, three different runs from the CST experiments are selected and surface scatterings are compared at frequencies near 500 Hz. Table 1 shows a summary of the selected runs. Although, CST7 (3C), CST7 (16G), and CST7 (25*D*) tests were conducted under different environmental conditions, frequencies are chosen close to each other to compare the scattering results in the same source features. In this way, in addition to validation of the SSAS software, it is possible to examine a unique source under different environmental conditions.

Table 2 Source parameters in simulation of CST7 (3C)

Source pressure level in the range 1 m	Frequency	Incident angle
200 dB	510 Hz	0 deg

Required data from Table 1 are introduced to the computer code as input. The developed software analyzes the environmental condition and calculates the scattering strength in a defined source condition. Source pressure in the range of 1 m (Pa) is calculated according to the weight of explosive charge which is 1.8 kg in the CST experiments. The resulting scattering strengths from three mentioned CST7 tests and by Chapman-Harris (CH), perturbation theory, and optimized HKF methods are illustrated in Fig. 5.

As mentioned earlier, Ogden and Erskine [9] concluded that there are two different mechanisms in sound scattering. Figure 5a shows the results of the optimized HKF method and the CST7 (3C) experiment. According to the environmental conditions of CST7 (C3), wind speed is 15 m/s in sea state 4. Therefore, based on Fig. 5, this run is in CH region in which effects of the bubble population on the incident sound are dominant. Thus, it is reasonable to assume that values of the scattering strength by the optimized HKF and CST7 (C3) test approach that by CH 17.5 m/s curve. In Fig. 5b which is based on the CST7 (16G) run conditions, the optimized HKF and CST7 (3C) scattering strength values are almost equal to that of CH 17.5 m/s curve. Wind

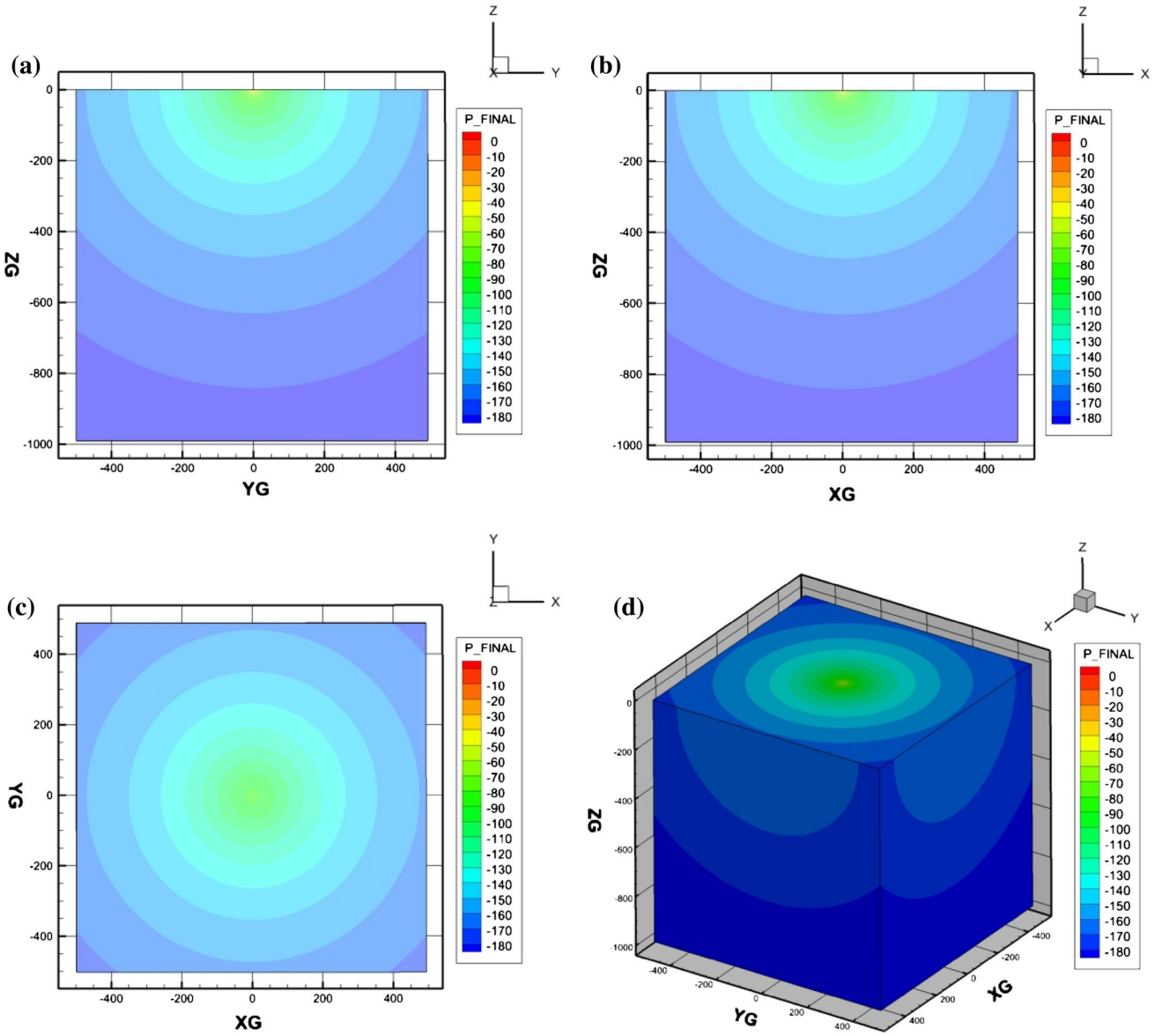

Fig. 8 Scattered pressure field (dB) in a domain of 1 km^3: **a** plane $x = 0$, **b** plane $y = 0$, **c** plane $z = -540$, **d** isometric view

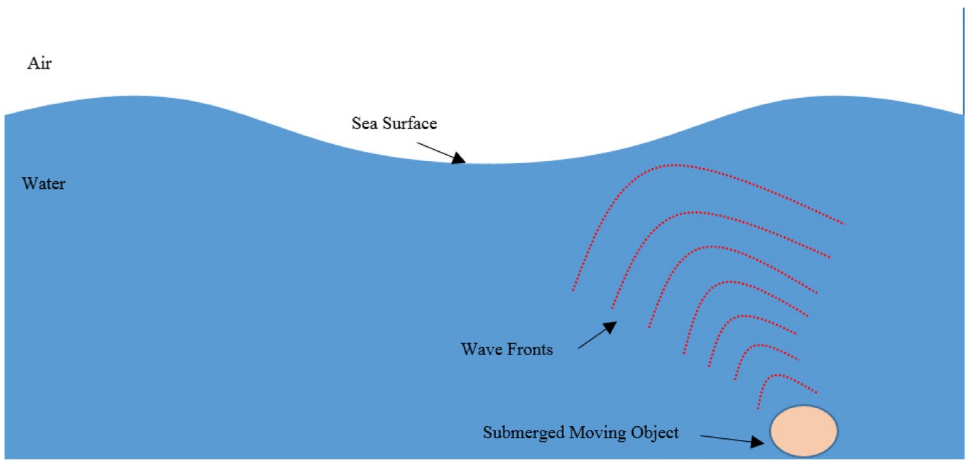

Fig. 9 Generated noise from a moving submerged object towards the sea surface

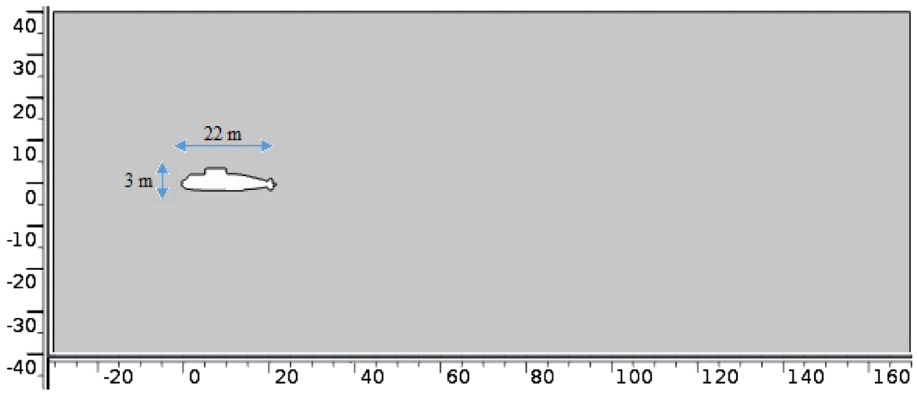

Fig. 10 The considered domain and size of the underwater robot

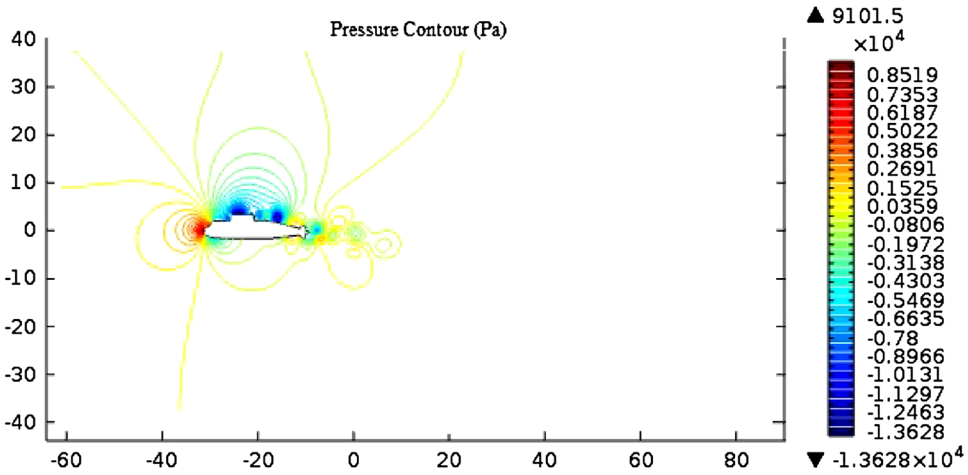

Fig. 11 Hydrodynamic pressure field around the robot

speed and frequency in CST7 (16G) experiment are in CH region (Fig. 5) and its sea state and wave height rms are higher than the CST7 (3C) test which shows that sub-surface bubbles can cause significant variations in scattering. This is indicative of the fact that they need to be included in the proposed models. In another word, due to breaking waves in high sea states which cause an increase in bubble population, the surface roughness has a minor role in the scattering strength. On the other hand, CST7 (25D) run conditions at 510 Hz frequency represents perturbation region (based on Fig. 5) in which surface roughness is dominant. As a result, it is reasonable to assume that the optimized HKF and CST7 (25D) curves tend to the perturbation curve.

The value of frequency is considered approximately constant in each run. Therefore, it is possible to examine the influence of other factors. In all runs, an increase in grazing angle causes a reduction in the absolute value of scattering strength. Also, when the wind speed increases due to an in increase in h_{rms} (Table 1 and Pierson–Moskwitz theory), the breaking waves and generated sub-surface bubble effects on the incident sound become dominant which result in the minor role of surface roughness. Therefore, in CST7 (25D) run which has the lowest wind speed among the selected runs, the results of optimized HKF method tend to those of the perturbation method which is reasonable.

4 Acoustic simulation in the case of explosion as a sound source

In the CST experiments, explosive charges are used as the sound source. The developed SSAS software is capable of simulating the explosion sound in the CST experiments. To conduct this simulation, the considered domain is discretized in spherical coordinates. The discretized domain is shown in Fig. 6. Each node in the considered domain represents the role of a hydrophone which observes the generated sound features in its coordinates. Based on the amount of explosive charges, the SSAS program simulates the propagation of explosion sound. Figure 7 shows how explosion sound propagates in a spherical domain.

As resulting wave fronts advance in the ocean, there are several boundaries such as sea floor, sea surface, and submerged bodies among others around it which can affect

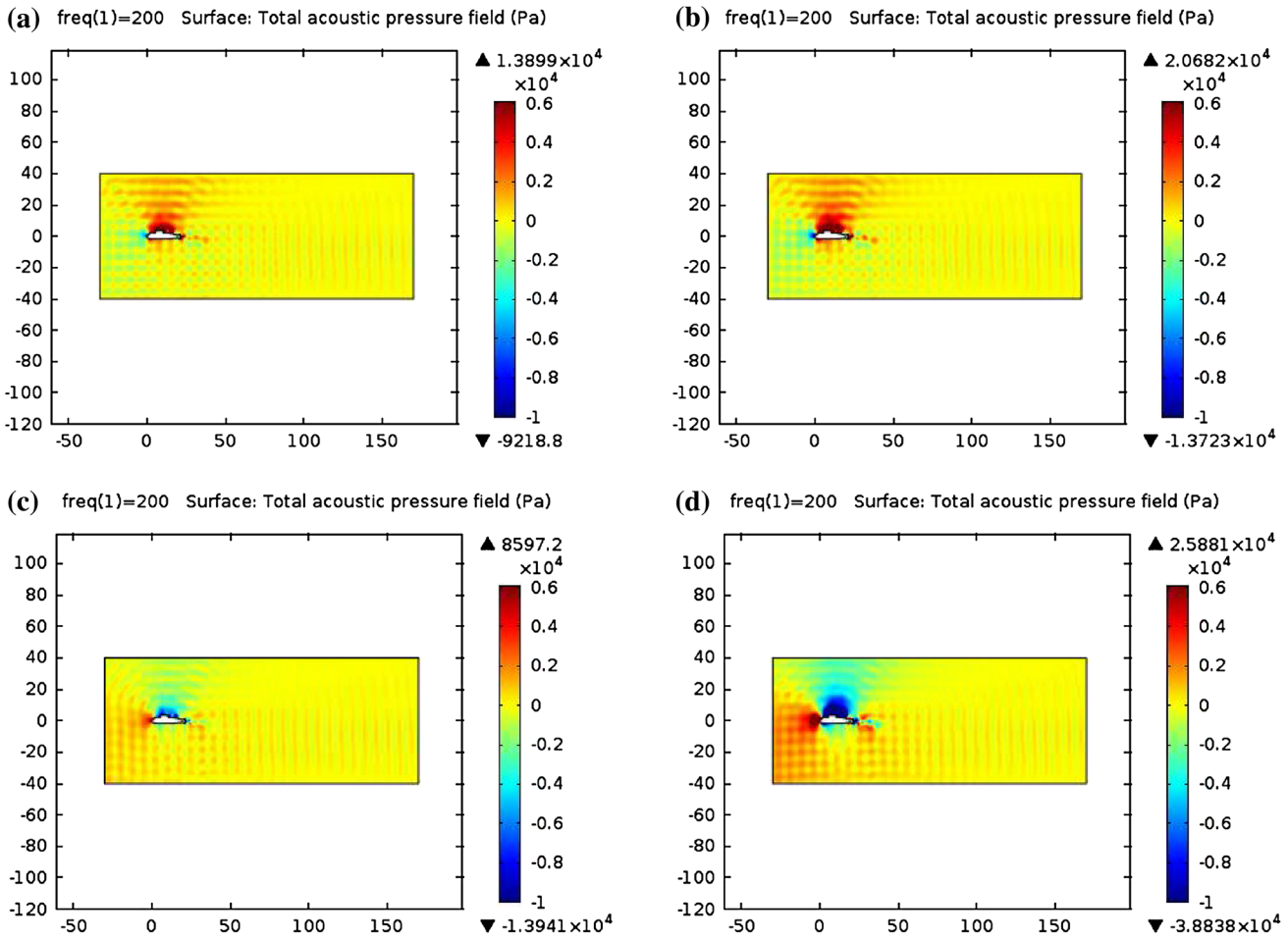

Fig. 12 Scattered acoustic pressure from the object ($f = 200$ Hz): **a** $\phi = 45°$, **b** $\phi = 9°$, **c** $\phi = 135°$, **d** $\phi = 180°$

the sound propagation. In this paper, simulation of the scattered acoustic pressure field (dB) from the sea surface is the main objective which is conducted by the SSAS program. To simulate this phenomenon, it is important to have enough information (such as Table 1) about the sea surface condition. Therefore, to simulate the surface scattering, the CST7 (3C) run conditions are selected. The explosion depth and sea surface information are shown in Table 1. Also, other important source parameters are needed for simulation of the scattered sound in the current run, which are shown in Table 2.

Generated sound hits the sea surface and based on the defined surface conditions, simulation of the sound scattering is conducted by the introduced computer code. The obtained scattered acoustic pressure field (dB) in a water domain (1 km^3) is shown in Fig. 8. Source pressure level in the range of 1 m and source depth are respectively, 200 dB and 540 m. In the current run, sea surface is at a middle sea state 4 and wind speed 15 m/s condition. Therefore, incident sound strikes a rough surface with a high population of sub-surface bubbles which are generated due to the breaking waves. As pointed out earlier, the scattering mechanism is divided into two regions and a transition part. Frequencies of the incident sound and wind speed over the sea surface are respectively, 500 Hz and 15 m/s. Hence, the incident sound will experience a mechanism close to CH. Therefore, because of energy loss due to the damping of bubbles cloud and value of the incident angle, sound will be scattered with lower pressure level and a symmetric profile based on the proposed optimized HKF method (Fig. 8). Similar profile for scattered sound in 2D is concluded by Urick [18]. Sound frequency is 510 Hz which is categorized as low frequency sound. So, the considered domain size of (1 km^3) is suitable for capturing the sound propagation.

5 Acoustic simulation in the case of a submerged moving object

Moving submerged objects generate hydrodynamic pressure which produces noise in water. The generated

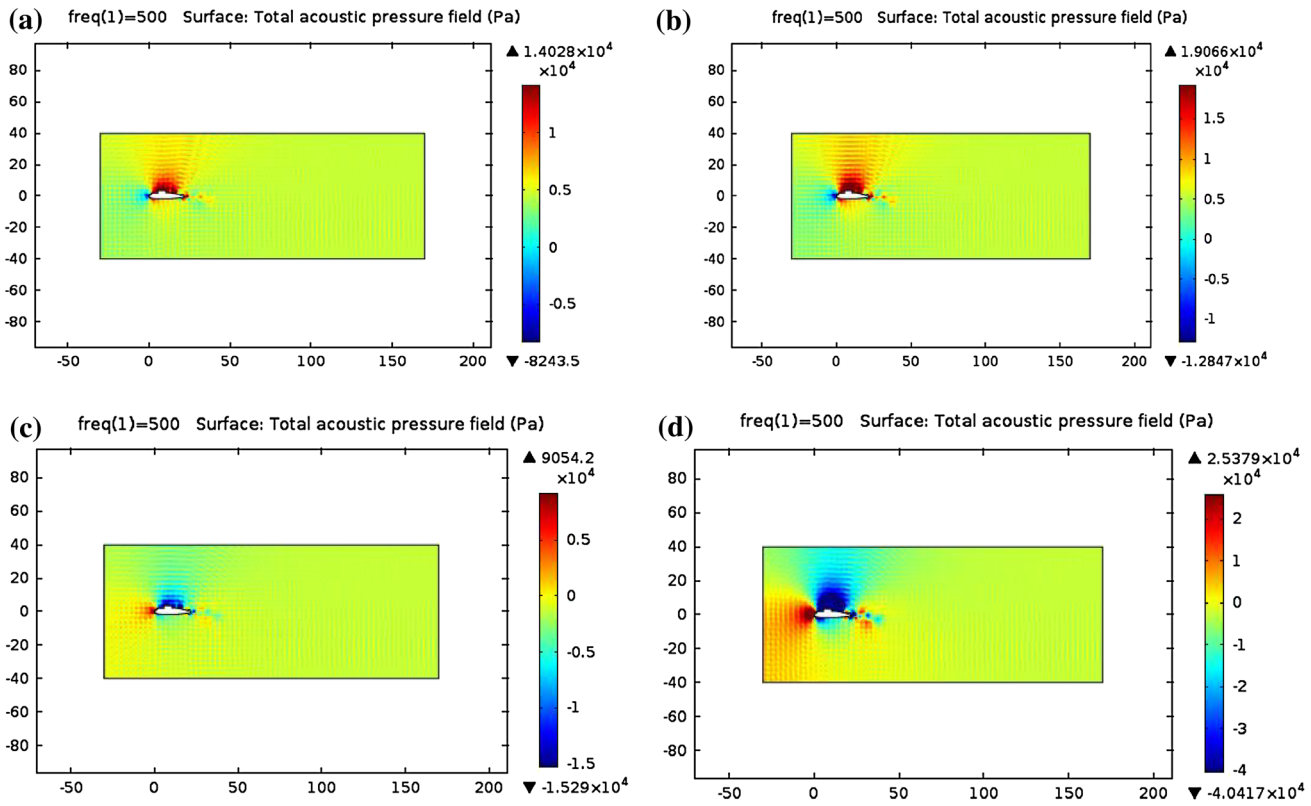

Fig. 13 Scattered acoustic pressure from the object ($f = 500$ Hz): **a** $\phi = 45°$, **b** $\phi = 9°$, **c** $\phi = 135°$, **d** $\phi = 180°$

noise will propagate in different directions. Based on the wave direction, a segment of the wave front strikes the sea surface (Fig. 9). Surface conditions and source features determine how sound will be scattered. In this section, an underwater robot is selected as a moving submerged body in the ocean. Domain and robot sizes are indicated in Fig. 10. Here, hydrodynamic pressure field is computed and analyzed in COMSOL Multiphysics 4.3 to measure the generated noise. The following Navier–Stokes equations are the governing equations for the considered incompressible viscous flow. Based on this equation, inertia, pressure, and viscous force are all in equilibrium.

$$\rho \frac{D\boldsymbol{u}}{Dt} = -\nabla p + \mu \, \Delta \boldsymbol{u} \tag{20}$$

Here, ρ is density, $\boldsymbol{u}$ is velocity vector, t is time, p is pressure, and μ is dynamic viscosity. Equation (20) is solved to find the pressure source around the object (Fig. 11).

When the pressure source around the object is determined, it is possible to calculate the hydrodynamic pressure in the range of 1 m from the object which is needed to find the incident pressure features. The generated waves are spread in different directions. To determine which nodes around the body are involved in the radiated pressure towards the sea surface, it is imperative to calculate the acoustic pressure field in the selected domain. Therefore, Helmholtz wave equation which itself is derived from the more fundamental equations of state (continuity and motion) is used to obtain the acoustic pressure field [1].

The Helmholtz wave equation is given as

$$\nabla . \frac{1}{\rho_c} (\nabla p_t) - \frac{K^2 p_t}{\rho_c} = 0 \tag{21}$$

where ρ_c is water density (kg/m^3), K is wave number which is defined as

$$K = \frac{\omega}{C_c} \tag{22}$$

Here, ω is angular frequency of the sound (rad/sec), and C_c is the sound speed. Parameter p_t in Eq. (21) represents the total fluid pressure in the domain and is defined as

$$p_t = p_{\mathrm{A}} + p_b \tag{23}$$

where p_{A} is the ambient pressure which is equal to the hydrostatic pressure, and p_b is the calculated hydrodynamic pressure from Eq. (20). Therefore, through Eq. (21), it is possible to obtain the scattered acoustic pressure from the object.

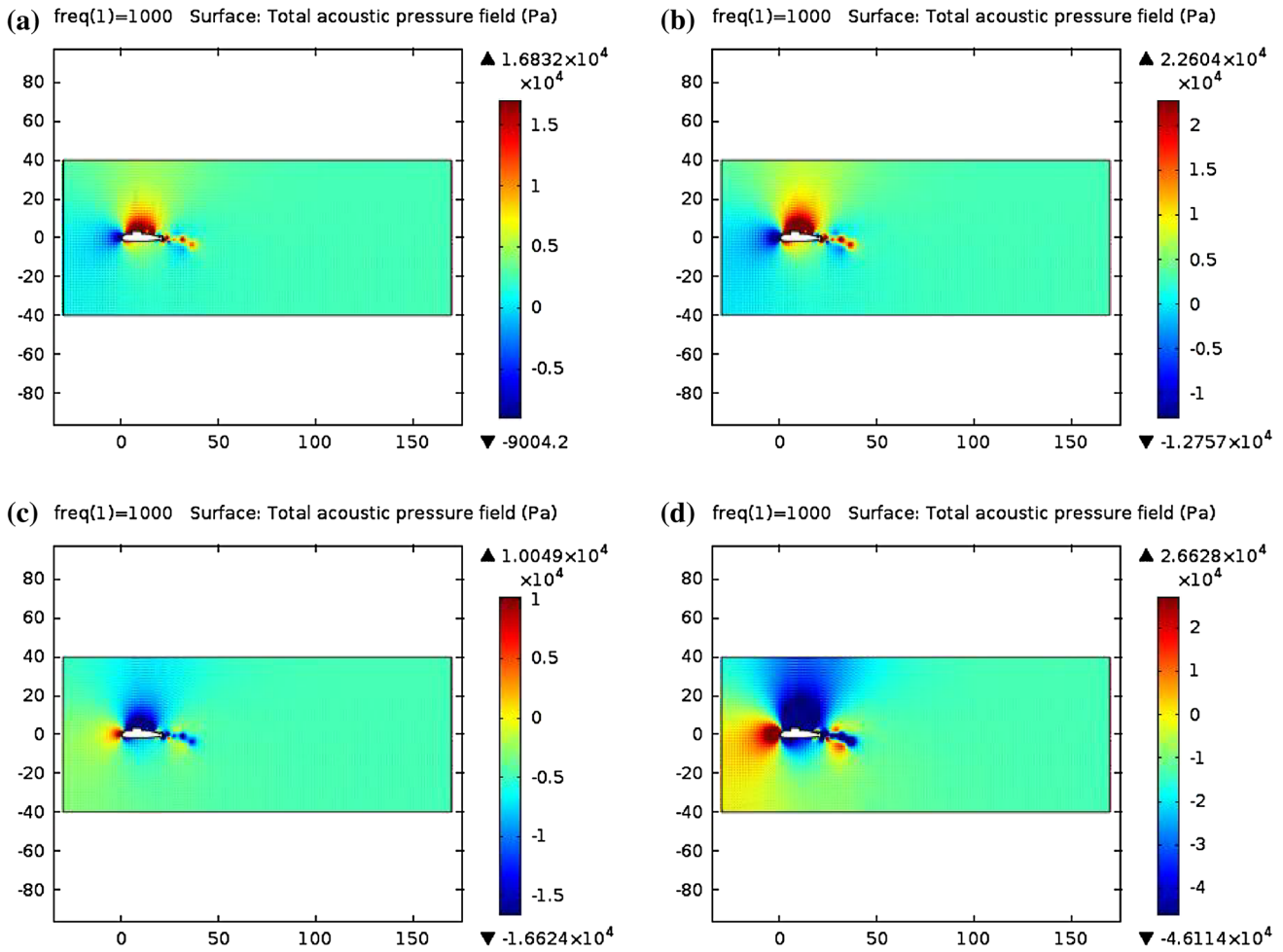

Fig. 14 Acoustic scattered pressure from the object ($f = 1{,}000$ Hz): **a** $\phi = 45°$, **b** $\phi = 9°$, **c** $\phi = 135°$, **d** $\phi = 180°$

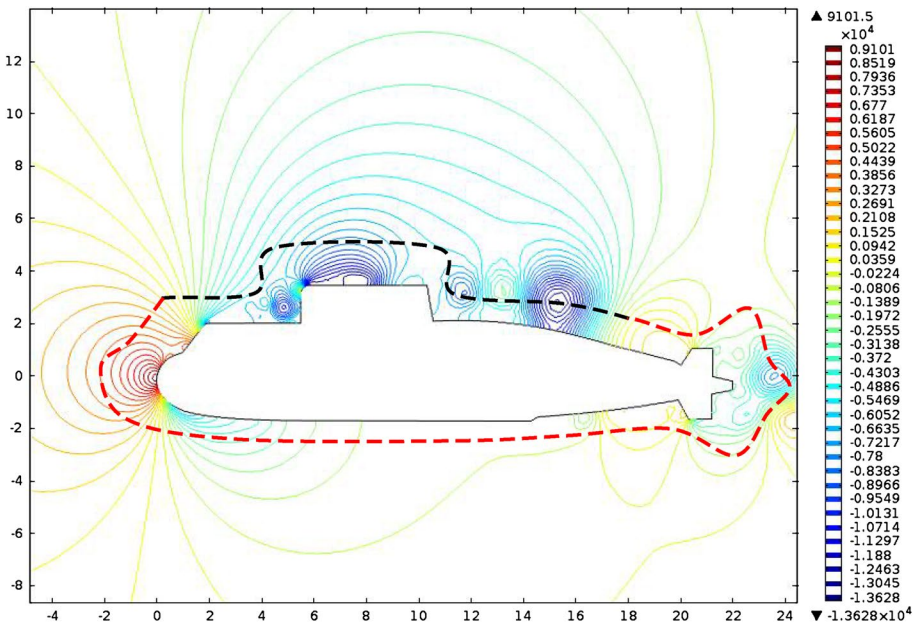

Fig. 15 Closed-curve around the object

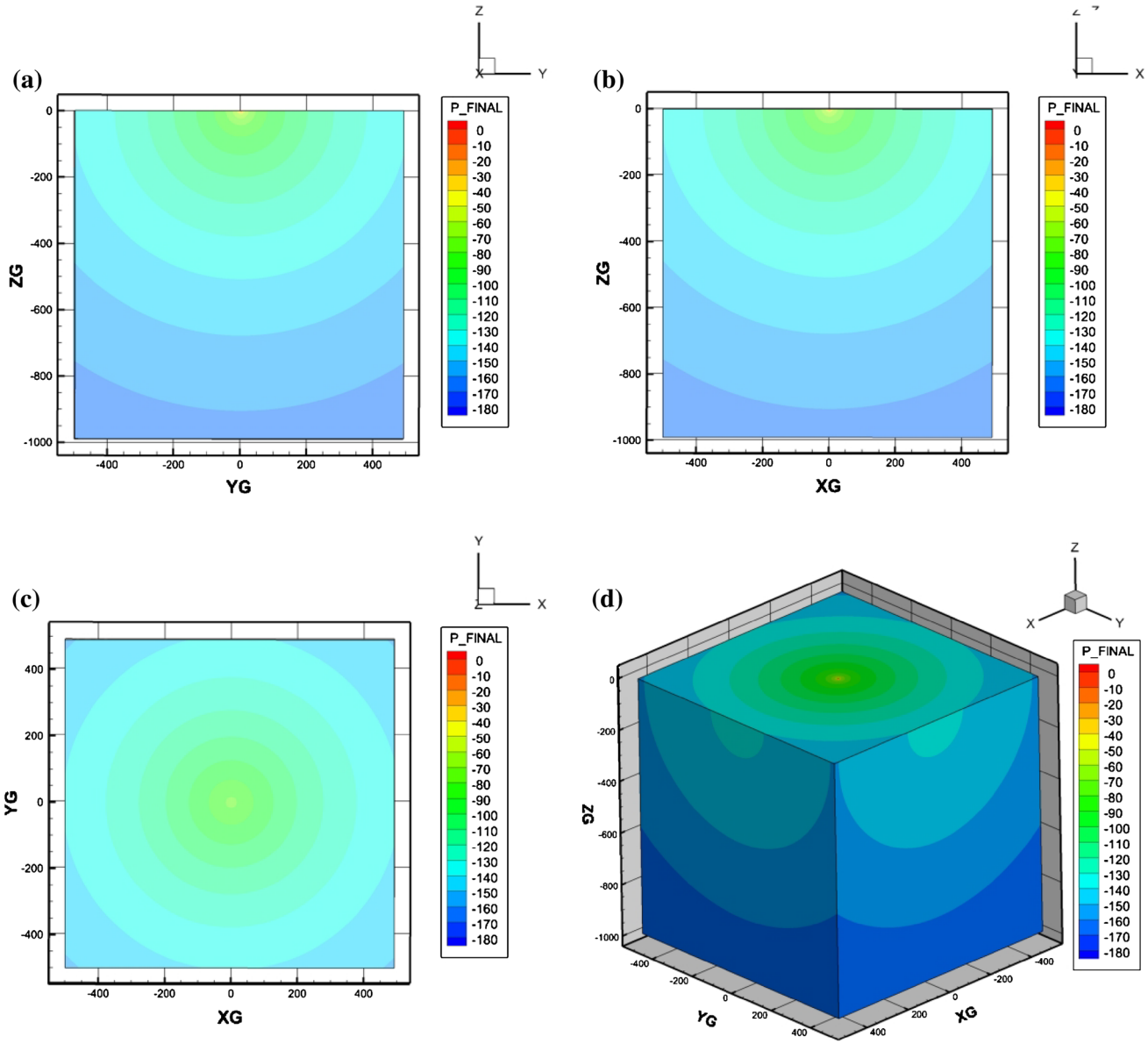

Fig. 16 Scattered pressure field (dB) from the sea surface at frequency 200 Hz: **a** plane $x = 0$, **b** plane $y = 0$, **c** plane $z = -40$, **d** isometric view

It should be pointed out that sound source frequency is required as an input for an acoustical analysis in Comsol software. However, this sound source frequency is not achievable in the hydrodynamic analysis of the Comsol and must be inputed to the acoustics solver of Comsol. Therefore, to perform the calculations quantitatively, three different frequencies in the low frequency range (200, 500, 1,000 Hz) are chosen to propagate the generated sound in the designated domain. Since the speed of the object is considered constant (5 m/s), hydrodynamic pressure field is the same in all three cases. The scattered pressure fields from the object in different phases are illustrated in Figs. 12, 13, 14.

It is observed in Figs. 12, 13, 14 that the scattered pressure from the object propagates towards the sea surface with incident angle 0°. To obtain the source pressure in the range of 1 m which represents the sound source level, an imaginary closed-curve is considered around the object (Fig. 15) and hydrodynamic pressure on this curve is calculated. Based on Figs. 12, 13, 14, it is quite evident that pressure sources around the robot turret generate noise which propagates towards the sea surface. The mean value of hydrodynamic pressure on an arc of the closed-curve which covers the turret is calculated and used as source pressure in the range of 1 m from the object. The black dashed line in Fig. 15 represents more effective nodes from

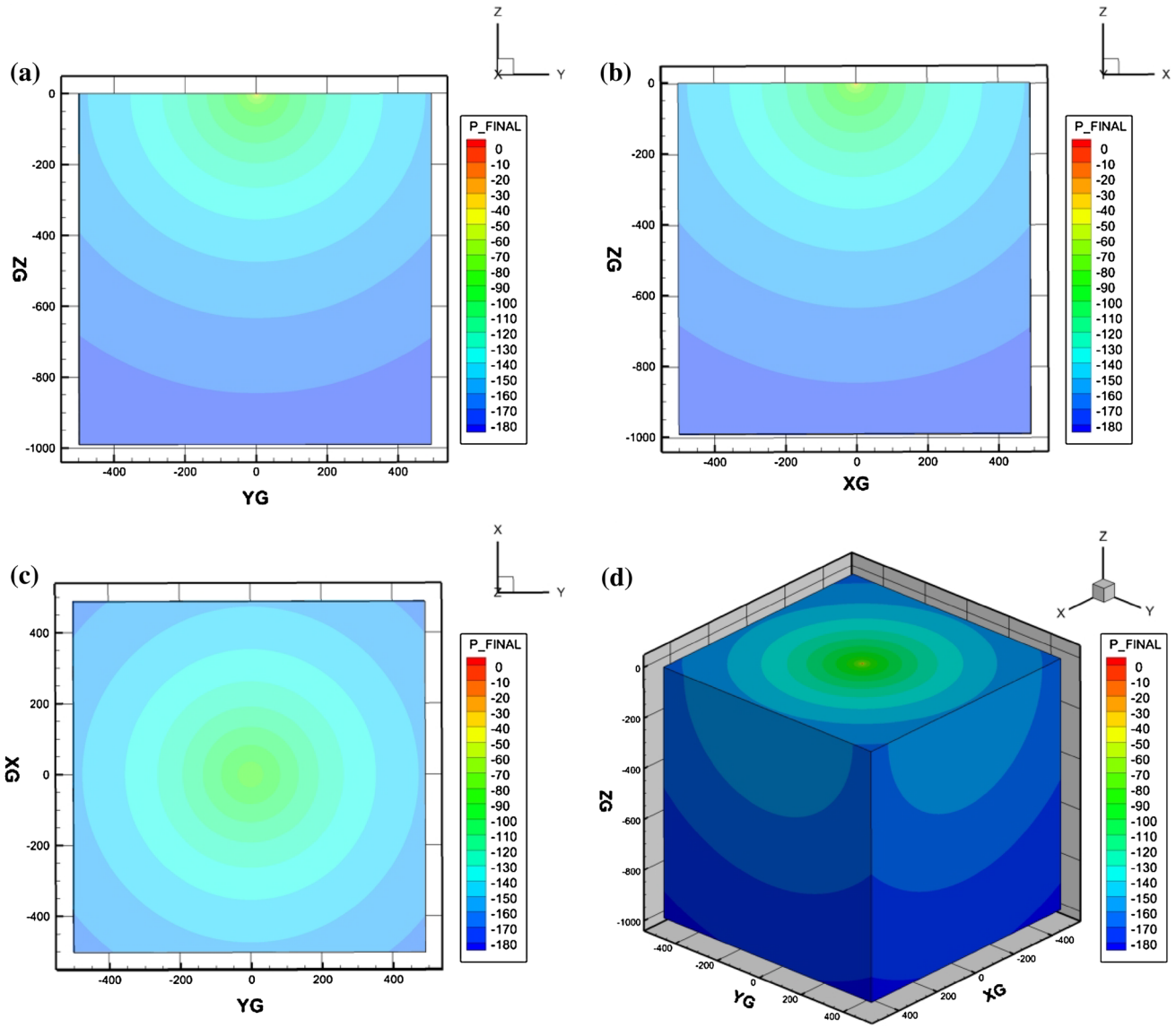

Fig. 17 Scattered pressure field (dB) from the sea surface at frequency 500 Hz: **a** plane $x = 0$, **b** plane $y = 0$, **c** plane $z = -40$, **d** isometric view

which the sound propagates towards the sea surface. The mean value of hydrodynamic pressure on the black dashed-line is found to be 0.712 Pa for the current run which is 117 dB in water.

The developed SSAS software needs the source features to analyze the scattered sound from the sea surface. The frequency (Hz), incident angle (degrees), source location, and source pressure (Pa) in the range of 1 m are the input source-dependent values for the SSAS computer code which are known for the current run.

As stated earlier, the developed code requires the sea surface condition for analyzing the scattered pressure from the sea surface. Sea surface features for the CST7 (C3) run are considered as surface condition for obtaining the scattered sound, as shown in Table 1. It is now possible to use the SSAS software to calculate the scattered acoustic pressure field. Scattered pressure fields from the sea surface calculated by the program for the three considered frequencies are displayed in Figs. 16, 17, 18.

The object position is X (0, 0, −40) in all three considered cases (Figs. 16, 17, 18). Scattered pressure field (dB) in three planes crossing the object location are shown in contour plots of (a), (b), and (c) in Figs. 16, 17, 18. To obtain the mentioned contours, accuracy of the scattering strength is checked at the source position and then extended to other nodes in the field. The scattered pressure profiles (dB) are similar to the patterns given by Medwin and Clay [19]. Although their relation considers the wind speed and

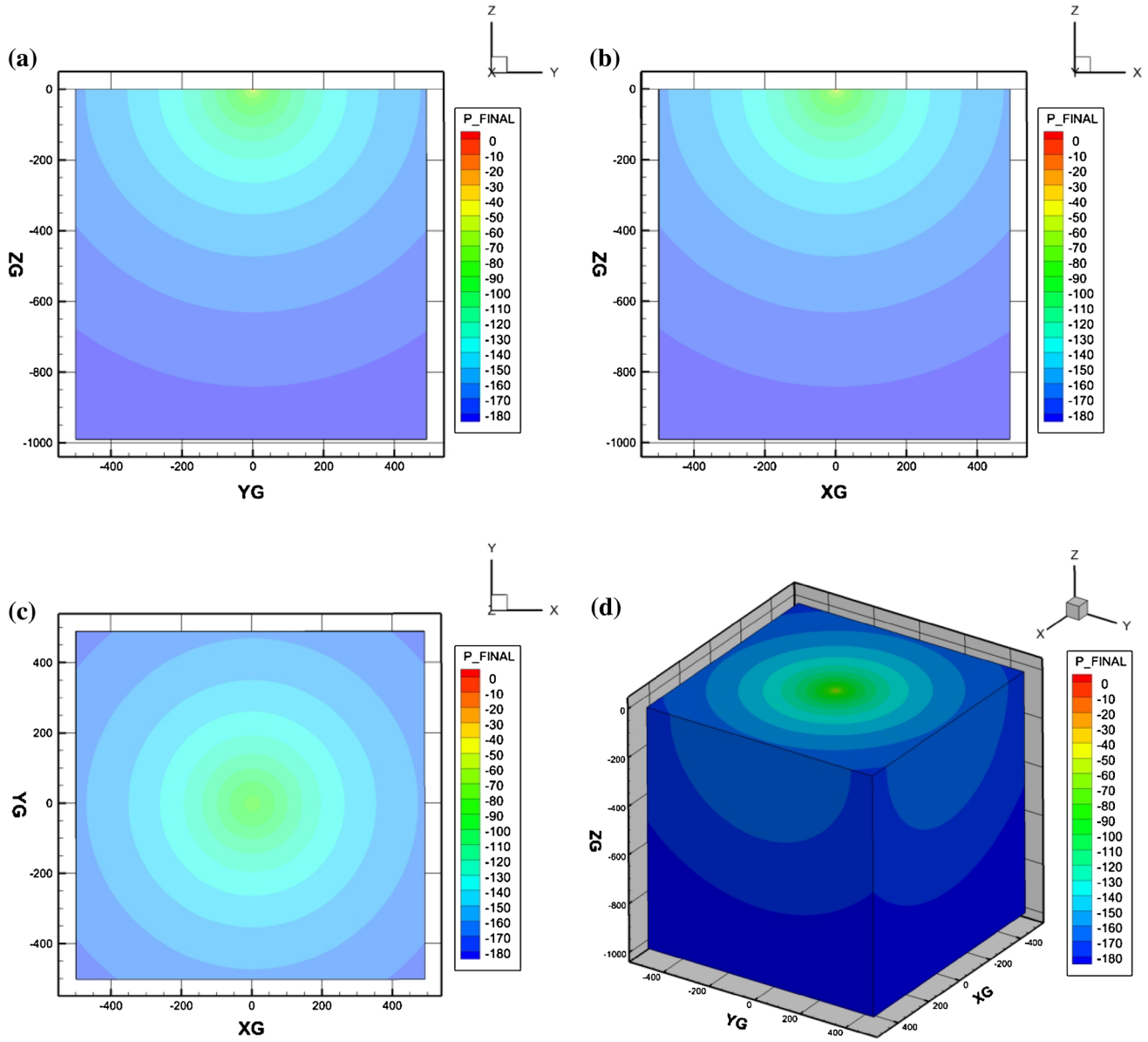

Fig. 18 Scattered pressure field (dB) from the sea surface at frequency 1,000 Hz: **a** plane $x = 0$, **b** plane $y = 0$, **c** plane $z = -40$, **d** isometric view

grazing angle as prime variables for the scattering phenomena, the suggested optimized HKF method includes additional frequency and subsurface bubble effects in its calculations which makes it more general and accurate. In Fig. 16 that correspond to 200 Hz frequency, the scattered pressure isosurfaces are wider than those at two higher frequencies in Figs. 17 and 18. Comparing the results of the scattered pressure for 500 Hz frequency (shown in Fig. 17) with the pressure isosurfaces at 1,000 Hz frequency (shown in Fig. 18) leads to the same conclusion. This conclusion seems accurate based on the reduction of the wave length quantity, as the frequency increases.

6 Conclusions

An optimized HKF method is proposed and a computer named SSAS is developed for simulating the scattering properties of incident sound from the sea surface. Scattered sound pressure level, sound intensity and scattering coefficient in different environmental conditions and source features are some outputs of this simulator.

Two different cases are considered as the sound sources. In the first case, particular runs of an experiment are considered. Accordingly, the generated sound due to an underwater explosion is simulated and the scattered sound from the

sea surface is analyzed. Due to the sea surface roughness and sub-surface bubble cloud, the incident sound exhibits energy loss and is scattered with less intensity in all directions. In the second case, the scattering of hydrodynamic noise which is generated by a moving submerged object is studied at low frequencies. The generated hydrodynamic pressure is calculated from the Navier–Stokes equations by the COMSOL Multiphysics software and is used in the Helmholtz equation to obtain the acoustic pressure field at three different frequencies. The generated wave pressure that propagates towards the sea surface is obtained and subsequently, the scattering from the sea surface corresponding to a particular experimental condition, is simulated by the developed software. The computational scattering results of the SSAS program are validated against other experimental runs in which limited number of hydrophones are used to observe the back-scattering strength. However, in all simulated cases, the scattered pressure field is calculated by the considered nodes which represent the role of hydrophones that can easily be increased in every direction. The acoustic simulations that are performed by the developed computer program based on the proposed optimized HKF method can be considered more economical compared to similar expensive experimental studies and can provide more analyzed and detailed information about sound scattering from the sea surface.

References

1. Etter PC (2003) Underwater acoustic modeling and simulation, 3rd edn. Spon Press, London, New York
2. Marsh HW (1961) Exact solution of wave scattering by irregular surfaces. J Acoust Soc Am 33:330–333
3. Kuo EYT (1988) Sea surface scattering and propagation loss: review, update, and new predictions. IEEE J Ocean Eng 13:229–234
4. Bass FG (1960) Boundary conditions for the average electromagnetic field on a surface with random irregularities and with impedance fluctuations. Izv Vuzov Radio Fizika 3:72–78
5. Brekhovskikh L, Lysanov Y (1982) Fundamentals of ocean acoustics. Springer, Berlin
6. Marsh HW, Schulkin M, Kneale SG (1961) Scattering of underwater sound by the sea surface. J Acoust Soc Am 33:334–340
7. Kuo EYT (1994) The perturbation characterization of reverberation from a wind-generated bubbly ocean surface-I: theory and a comparison of backscattering strength predictions with data. IEEE J Ocean Eng 19:368–381
8. Medwin H, Clay CS (1998) Fundamentals of acoustical oceanography, 2nd edn. Academic Press, Boston
9. Ogden PM, Erskine FT (1994) Surface scattering measurements using broadband in the explosive charges critical sea test experiments. J Acoust Soc Am 95:746–761
10. McDonald BE (1991) Echoes from vertically striated sub resonant bubble clouds: a model for ocean surface reverberation. J Acoust Soc Am 89:617–622
11. Henyey FS (1991) Acoustic scattering from ocean micro bubble plumes in the 100 Hz to 2 kHz region. J Acoust Soc Am 90:399–405
12. Medwin H (1974) Acoustic fluctuations due to micro bubbles in the near-surface ocean. J Acoust Soc Am 56:1100–1104
13. Prosperetti A, Lu NQ, Kim HS (1993) Active and passive acoustic behavior of bubble clouds at the ocean's surface. J Acoust Soc Am 93:3117–3127
14. Hall MV (1989) A comprehensive model of wind-generated bubbles in the ocean and predictions of the effects on sound propagation at frequencies Up to 40 kHz. J Acoust Soc Am 86:1103–1117
15. Gauss RC, Fialkowski JM (1993) Measurements of the spectral characteristics of low- frequency, low-grazing-angles surface reverberation. J Acoust Soc Am 93:2299 (A)
16. Medwin H, Kurgen A, Nystuen JA (1990) Impact and bubble sound from raindrops at normal and oblique incidence. J Acoust Soc Am 88:413–418
17. Ogden PM, Erskine FT (1994) Surface scattering measurements using broadband in the explosive charges critical sea test 7 experiments. J Acoust Soc Am 96:2908–2920
18. Urick RJ (1979) Sound propagation in the sea. Report # 19961226085, US Government Printing Office, Washington, DC
19. Medwin H, Clay CS (1964) High frequency acoustical reverberation from rough sea surface. J Acoust Soc Am 36:2131–2134